Available online at www.sciencedirect.com
ScienceDirect
Trans. Nonferrous Met. Soc. China 30(2020) 223−235
Transactions of Nonferrous Metals Society of China
www.tnmsc.cn

Separation of arsenic from arsenic−antimony-bearing dust through selective oxidation−sulfidation roasting with CuS

Da-peng ZHONG, Lei LI

State Key Laboratory of Complex Non-ferrous Metal Resources Clean Utilization,
Engineering Research Center of Metallurgical Energy Conservation and Emission Reduction of Ministry of Education,
Faculty of Metallurgical and Energy Engineering, Kunming University of Science and Technology,
Kunming 650093, China

Received 22 February 2019; accepted 1 December 2019

Abstract: The feasibility of a new method for separating arsenic from arsenic−antimony-bearing dusts using CuS was put forward, in which Sb was transformed into Sb_2O_4 and Sb_2S_3 that stayed in the roasted calcine while As was volatilized in the form of As_4O_6. The factors such as roasting temperature and CuS addition amount were studied using XRD, EPMA and SEM−EDS. CuS has an active effect on the separation of arsenic due to the destruction of $(Sb,As)_2O_3$ structures in the original dust and the simultaneous release of As in the form of As_4O_6. At a roasting temperature of 400 °C and CuS addition amount of 130%, the volatilization rates of arsenic and antimony reach 97.80 wt.% and 8.29 wt.%, respectively. Further, the high As volatile matter can be used to prepare ferric arsenate after it is oxidized, with this treatment rendering the vapor harmlessness.

Key words: arsenic−antimony-bearing dusts; separation of arsenic and antimony; CuS; phase transformation; waste utilization

1 Introduction

Arsenic−antimony-bearing dust is of great importance for recovering valuable metals as a secondary resource [1]. It is usually generated from the nonferrous metal smelting process and accumulates, resulting in high costs for landfill disposal and in the heavy pollution of water, land and air [2−5]. However, arsenic−antimony-bearing dust generally contains not only approximately 30 wt.% of antimony but also other abundant valuable metals, such as zinc, lead, copper, and bismuth [6−8]. The high arsenic content dust cannot be directly recycled into the antimony smelting process since the As−Sb alloys might be generated due to their similar chemical properties.

Arsenic and antimony in arsenic−antimony-bearing dusts exist mainly in the forms of As_2O_3 and Sb_2O_3, respectively, and they are difficult to be separated due to their similar physical and chemical properties [9,10]. The conventional treatment of arsenic−antimony-bearing dusts can be classified into three methods: hydrometallurgical, physical filtration and pyrometallurgical processes. In the hydrometallurgical process, arsenic can be selectively leached into solution and separated from antimony using acid [11,12], alkali [13−15], chlorination [16] or pressure leaching (in form of Na_3AsO_4) [10,17], and antimony is transformed into insoluble matter and further concentrated by filtration [14,18−20]. The arsenic removal rate can reach 92 wt.% in the hydrometallurgical process [10,13−17], but the arsenic-containing

Foundation item: Project (51564034) supported by the National Natural Science Foundation for Distinguished Regional Scholars, China; Project (2015HA019) supported by the Scientific and Technological Leading Talent Program in Yunnan Province, China

Corresponding author: Lei LI; Tel: +86-13987619187; E-mail: tianxiametal1008@163.com

DOI: 10.1016/S1003-6326(19)65194-0

wastewater generated from this process poses a potential threat to the environment. Based on the high-temperature filtration technology, a cleaner and more effective method of physical filtration was investigated by ZHANG et al [21]. Approximately 92.24 wt.% of arsenic was removed at the expense of the loss of 6−7 wt.% of antimony in their studies. However, the porous FeAl(20Cr) intermetallic filter materials used to separate As were seriously corroded by the high-temperature As-containing gas, causing it difficulty for industrial application. As_2O_3 was easy to volatilize, and its volatilization rate exceeded 93.0 wt.% at 460 °C for 120 min [22]. The Sb_2O_3 volatilization also exceeded 95.0 wt.% at 600 °C for 120 min under a nitrogen atmosphere [23]. When the oxygen partial pressure exceeded 10 vol.%, PADILLA et al [24] found that Sb_2O_3 volatilization was seriously inhibited by the formation of a non-volatile compound, SbO_2. The arsenic could be separated effectively if Sb_2O_3 was selectively oxidized from As_2O_3 and Sb_2O_3 to SbO_2 in a suitable oxidizing atmosphere. Thus, a roasting process in a selectively oxidizing atmosphere using O_2 for treating high As−Sb dusts was investigated by LI et al [9] and TANG et al [25], but their studies showed that only approximately 60 wt.% of arsenic was removed and that the antimony lost was greater than 10 wt.%. The reason might have been that As_2O_3 and Sb_2O_3 were combined and transformed into a solid solution phase, $As_xSb_yO_6$ (where x=1, 2 or 3, and $x+y$=4), during the roasting process, which inhibited the volatilization of arsenic and simultaneously promoted the volatilization of antimony at 200−800 °C [26−28]. Meanwhile, As_2O_3 could be oxidized to As_2O_5 under an O_2 atmosphere, which also restricted the volatilization of arsenic. Thus, ZHONG et al [29] proposed a method using CuO as a weak oxidant to treat this dust. The solid solution phase $As_xSb_yO_6$ was effectively destroyed by CuO, in which the Sb component was selectively oxidized to Sb_2O_4 and As was transformed to As_4O_6 and volatilized. In their research, the arsenic removal rate reached 91.50 wt.% but was accompanied by an antimony loss rate of 8.63%.

In the study by PADILLA et al [24], the stibnite (Sb_2S_3) volatilization rate did not exceed 20 wt.% at a roasting temperature of 700 °C, roasting time of 60 min and N_2 flow rate of 1.5 L/min, indicating that the stibnite (Sb_2S_3) volatility is far lower than that of Sb_2O_3. Combined with the low volatility of stibnite (Sb_2S_3) and weak oxidizability of Cu^{2+}, a new method of selective oxidation−sulfidation for treating arsenic−antimony-bearing dusts was put forward. CuS was used as an additive in the roasting process, and the influences of processing parameters on separating arsenic were investigated, including the roasting temperature and amount of CuS addition.

2 Experimental

2.1 Materials

The arsenic−antimony-bearing dust used in this study was provided by a plant for treating tin anode slime using the pyrometallurgical process; the plant is located in Yunnan Province, China. The chemical composition (wt. %) of the dust is presented in Table 1, which shows that the major elements present are arsenic (36.28 wt.%), antimony (28.72 wt.%) and oxygen (21.73 wt.%). The "Others" in Table 1 are mainly Ca, K, and Si, etc. The XRD pattern of this arsenic−antimony-bearing dust is reported in Fig. 1(a), which shows that the main phases are As_2O_3 and Sb_2O_3, accompanied by a small amount of $(Sb,As)_2O_3$ solid solution [28]. Furthermore, As_2O_3 holds a more content than Sb_2O_3 in coexistent states of As−Sb−O seen from compositions of points 2, 3 and 5 (Fig. 1(b)) in Table 2, which implies that the formation of this solid solution is through the dissolution of Sb_2O_3 into As_2O_3. In addition, the dust contains tiny amounts of Cu and S in Table 2, which agrees with the result in Table 1.

Table 1 Chemical composition of arsenic−antimony-bearing dust (wt.%)

As	Sb	O*	C	Se	Pb	F
36.28	28.72	21.73	2.52	2.46	2.06	2.05
Fe	Bi	Na	Sn	Cu	S	Others
1.13	0.68	0.40	0.25	0.24	0.20	1.28

*Data obtained from LECO TC-600 nitrogen/ oxygen analyzer

CuS prepared via a precipitation process was used as an additive. It was of analytical grade (purity of 99%) and was procured from local suppliers. In addition, the high purity N_2 (purity of

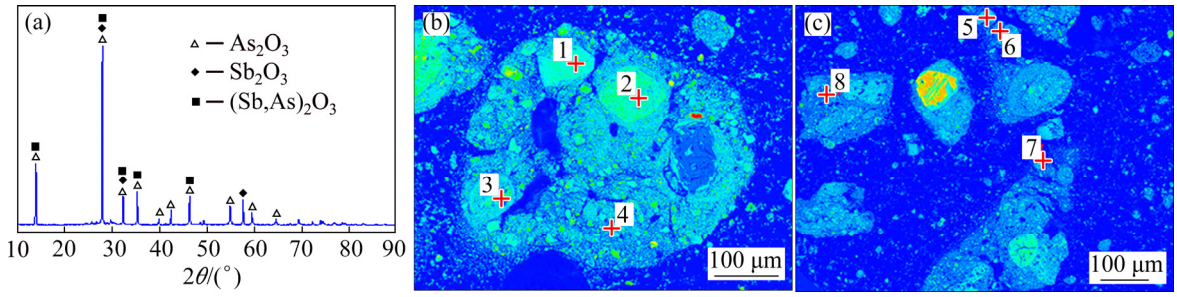

Fig. 1 XRD pattern (a) and EPMA images (b, c) of arsenic−antimony-bearing dust

Table 2 Elemental analysis of different phases (wt.%)

Point	NaO	As_2O_3	SiO_2	SO_3	FeO	CuO	TeO_2	Sb_2O_3	Cr_2O_3	PbO	Possible phase
1	0	98.798	0.248	0.130	0.004	0.077	0	0.31	0.149	0.006	As−O
2	0.06	56.302	0.103	0.175	1.932	0	0	40.091	0.213	0.306	As−Sb−O
3	0.054	55.493	0.013	0.167	3.267	0.032	0	40.208	0.071	0.667	As−Sb−O
4	0	98.455	0.149	0	0.042	0.014	0	0.184	0	0	As−O
5	0.107	74.806	0.264	0.129	0.086	0.09	0	22.486	0.541	1.646	As−Sb−O
6	0.056	3.336	0	0.042	0.042	0	0	95.183	0.303	0.08	Sb−O
7	0	98.093	0.013	0.146	0.006	0.026	0	0.877	0	0.069	As−O
8	0.049	3.001	0	1.631	0	0.071	0	94.142	0.064	0.829	Sb−O

99.999%) used was also procured from local suppliers.

2.2 Methods

The experimental apparatus is shown in Fig. 2. An appropriate amount of CuS was first mixed adequately with 5 g arsenic−antimony-bearing dust in the experiment. The addition amount of CuS added (α) was calculated using Eq. (1):

$$\alpha = \frac{m_C}{m_D} \times 100\% \quad (1)$$

where m_C and m_D stand for the mass of CuS added and arsenic−antimony-bearing dusts, respectively. The mixture then was put into a corundum crucible and roasted in a tube furnace (Fig. 2) at the required temperature for the proper time under a nitrogen atmosphere. The off-gas from the reaction tube was continuously passed through a water-cooled condenser, which collected the volatile matter, and then to solutions of 1 mol/L NaOH to remove harmful components. Finally, after holding for a proper time, the roasted calcines were weighed, ground and chemically analyzed to investigate the volatilization rates of arsenic and antimony.

2.3 Characterization

The thermogravimetric analysis (TG) and differential scanning calorimetry (DSC) of the samples were performed in a thermal analyzer (NETZSCH, STA 449 F3). Typical measurements were performed at a heating rate of 0.167 K/s under N_2 atmosphere. The X-ray diffraction analysis (XRD, Rigaku, TTR-III) and electron probe microanalysis techniques (EPMA, JXA82, JEOL) coupled with an energy dispersive spectrometer (EDS) were used to detect phase transformations and the morphology of the samples during the roasting process, and the chemical compositions of the samples were characterized by chemical analysis. Specifically, the O content in the original dust was characterized by LECO TC−600 nitrogen/oxygen analyzer. The phase contents in the roasted calcines were calculated through K value method. The FactSage 7.0 software was used to calculate the standard Gibbs free energy changes and equilibrium compositions of the reaction system. Mathematical expressions of the volatilization rates of arsenic (R_{As}) and antimony (R_{Sb}) were defined as follows:

$$R_{As} = \left(1 - \frac{m_T w_{As2}}{m_D w_{As1}}\right) \times 100\% \quad (2)$$

$$R_{Sb} = \left(1 - \frac{m_T w_{Sb2}}{m_D w_{Sb1}}\right) \times 100\% \quad (3)$$

where m_D and m_T stand for the masses of the original arsenic−antimony-bearing dust and roasted calcines respectively; w_{As1} and w_{Sb1} are the arsenic

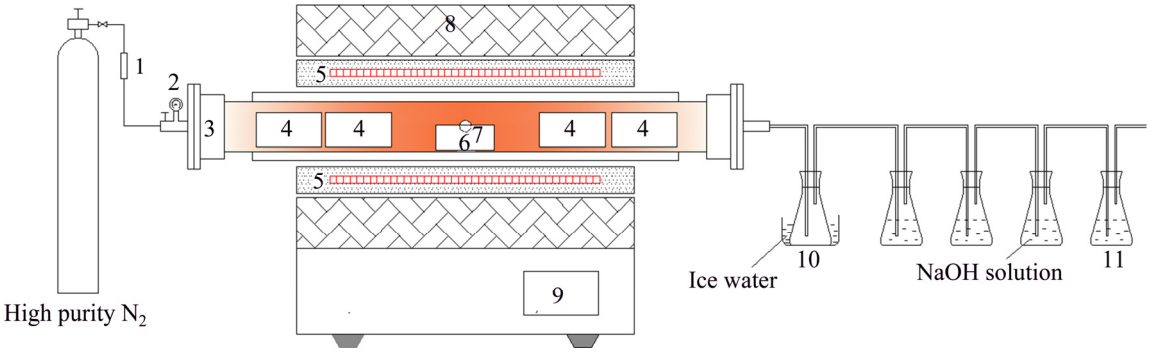

Fig. 2 Experimental setup: 1—Flowmeter; 2—Pressure valve; 3—Furnace cover; 4—Furnace plug; 5—Silicon carbide bar; 6—Corundum boat; 7—Thermocouple; 8—Electric furnace; 9—Control cabinet; 10—Water-cooled condenser; 11—Alkali vessel

and antimony contents in the original arsenic−antimony-bearing dust, respectively; and w_{As2} and w_{Sb2} are the arsenic and antimony contents in the roasted calcines, respectively.

3 Thermo-chemical behavior

Figure 3 shows the TG−DSC curves of CuS, arsenic−antimony-bearing dusts and their mixture (α=130%) under an N_2 atmosphere. Two endothermic peaks located at 262.2−470.5 °C are detected in the DSC measurement for the arsenic−antimony-bearing dusts, and each corresponds to a mass loss. The first endothermic peak at 262.2−289.7 °C is attributed to the As_2O_3 phase melting (the melting point of As_2O_3 is 275 °C) [30] and dust volatilization. The second peak at 415.6−470.5 °C is attributed to evaporation of the dust. As reported in Ref. [27], As_2O_3 begins to volatilize at 200 °C and its volatilization rate increases to approaching 100 wt.% at 500 °C, which corresponds the first endothermic peak in the DSC curves of dust in Fig. 3. Sb_2O_3 begins to volatilize at 500 °C, and its volatilization rate increases to 80 wt.% at 800 °C. In addition, the volatilization rate of the mixture of As_2O_3 and Sb_2O_3 (solid solution, $As_xSb_yO_6$) increases from 0 to 54.3 wt.% at 200 to 350 °C, remains nearly constant at 520 °C, and finally continues to increase with the increase of temperature. The volatilization of As_2O_3, Sb_2O_3 and mixture of them results in the second peak in the DSC curves of dust in Fig. 3. The main evaporation processes are shown in Eqs. (4)−(6). There are seven endothermic peaks in the DSC curves of CuS, and each of these peaks corresponds to a mass loss.

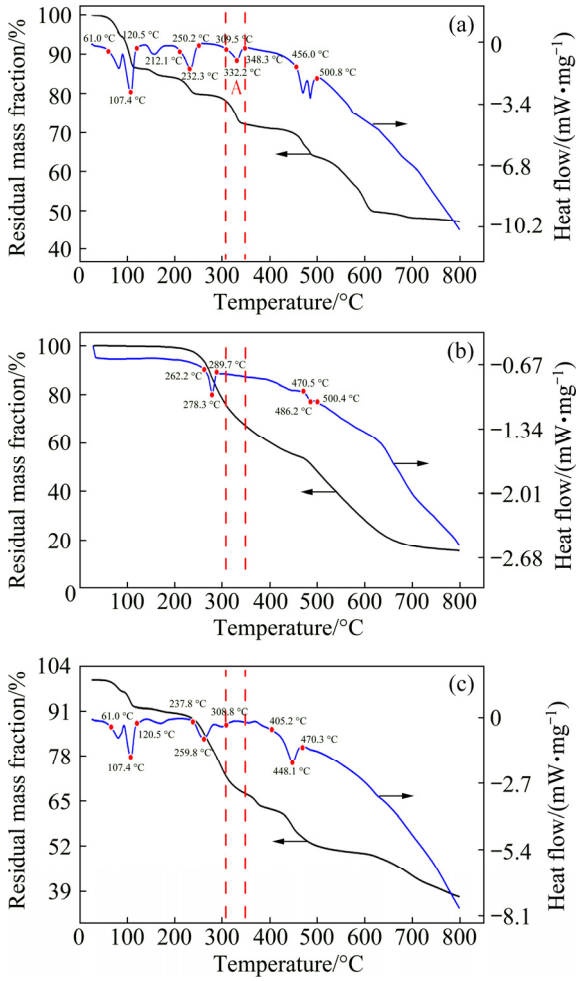

Fig. 3 TG−DSC curves of CuS (a), arsenic−antimony-bearing dust (b) and their mixture (α=130%) (c)

The first endothermic peak at 61.0−120.5 °C is attributed to the evaporation of free water, and the other endothermic peaks are attributed to the gradual decomposition of CuS as shown in Eq. (7) (where $1<z\leq2$), in which the decomposition

products might be Cu_9S_8, Cu_7S_4, $Cu_{1.8}S$, and Cu_2S [31,32]. Compared with the DSC curves of individual CuS and arsenic−antimony-bearing dusts, no new endothermic or exothermic peak is observed at 25−309.5 °C for the mixture of them seen from Fig. 3, indicating that no reaction occurs between the dust and CuS in this temperature range. Concretely, the first endothermic peak at 61.0−120.5 °C is attributed to the evaporation of free water, and the endothermic peak at 212.1−250.2 °C is attributed to the As_2O_3 phase melting, gradual decomposition of CuS and dust volatilization. When the temperature is increased to 309.5−348.3 °C, no peak is observed in the DSC curve for the mixture, which differs from the curve of CuS. Specifically, in the DSC curve of CuS, an endothermic peak A centered at 332.2 °C can be observed. This difference might be attributed to the occurrence of an exothermic reaction between the dust and CuS and/or the decomposition products of CuS. Figure 4(a) shows that Eq. (8) can be carried out, and Fig. 4(b) shows that Eq. (8) is an exothermic reaction. Due to the lack of the thermodynamic data for the decomposition products of CuS, Cu_9S_8, Cu_7S_4, and $Cu_{1.8}S$, the standard Gibbs free energy changes of those reactions between them and the dust are not shown in Fig. 4. With a further increase in temperature, an obvious endothermic peak is observed at 405.2−470.3 °C, which might be related to the occurrence of Eqs. (9)−(13). Equation (9) cannot occur due to its positive standard Gibbs free energy in Fig. 4(a). Furthermore, the standard Gibbs free energy values of Eqs. (10) and (12) are more negative than those of Eqs. (11) and (13) at above 200 °C, which means that the sulfidation of Sb_2O_3 is carried out prior to that of As_2O_3 and that the selective sulfidation of Sb_2O_3 could be realized. Besides, there is some $(Sb,As)_2O_3$ solid solution existing in the original dust seen from Fig. 1, in which the arsenic trioxide might have some affinity with antimony tetroxide and further influences the oxidation and sulfidation of Sb_2O_3. These solid solutions were assumed as ideal solid solution in this study, whereas arsenic trioxide was assumed to have less affinity with antimony tetroxide and thus Sb_2O_3 has a higher activity coefficient according to the Raoult's law (activity coefficient γ=1). The thermodynamic calculation results, presented in Fig. 5, demonstrate that the formation of these solid solutions restricts the oxidation of Sb_2O_3 to Sb_2O_4 or the formation of Sb_2S_3 obviously.

$$Sb_2O_3(s)=1/2Sb_4O_6(g) \quad (4)$$

$$As_2O_3(s)=1/2As_4O_6(g) \quad (5)$$

$$(Sb,As)_2O_3(s)\rightarrow As_xSb_yO_6(g) \quad (6)$$

$$CuS(s)\rightarrow Cu_2S(s)+S(s,l) \quad (7)$$

$$CuS(s)+2/3Sb_2O_3(s)= 1/2Cu_2S(s)+1/2Sb_2O_4(s)+1/6Sb_2S_3(s) \quad (8)$$

$$CuS(s)+5/12As_2O_3(s)= 1/2Cu_2S(s)+1/4As_2O_5(s)+1/6As_2S_3(s) \quad (9)$$

$$CuS(s)+1/9Sb_2O_3(s)= 1/2Cu_2S(s)+1/6SO_2(g)+1/9Sb_2S_3(s) \quad (10)$$

$$CuS(s)+1/9As_2O_3(s)= 1/2Cu_2S(s)+1/6SO_2(g)+1/9As_2S_3(s) \quad (11)$$

$$S(s,l)+2/9Sb_2O_3(s)=1/3SO_2(g)+2/9Sb_2S_3(s) \quad (12)$$

$$S(s,l)+2/9As_2O_3(s)=1/3SO_2(g)+2/9As_2S_3(s) \quad (13)$$

FactSage 7.0 was used to calculate the equilibrium phases for the roasted products by minimizing Gibbs free energy under isothermal, isobaric and fixed-mole conditions. The required data for computation were provided by the FactPS database of the program.

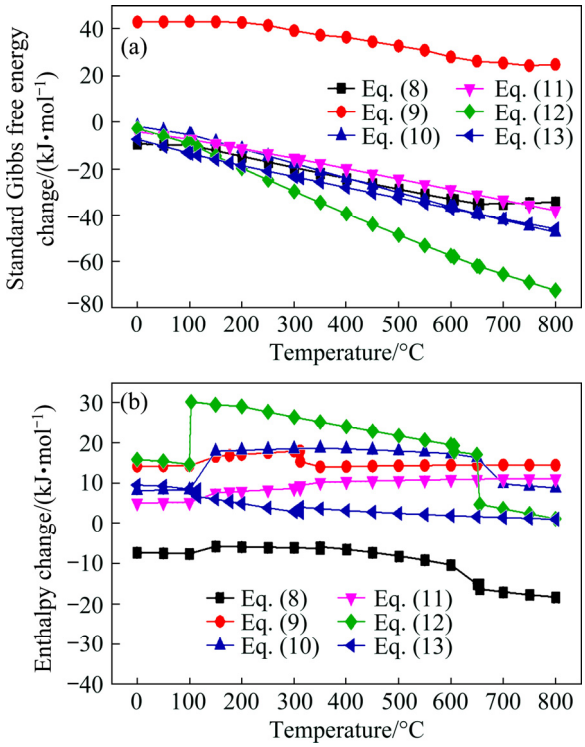

Fig. 4 Standard Gibbs free energy changes (a) and enthalpy changes (b) of Eqs. (8)−(13) in temperature range of 0−800 °C

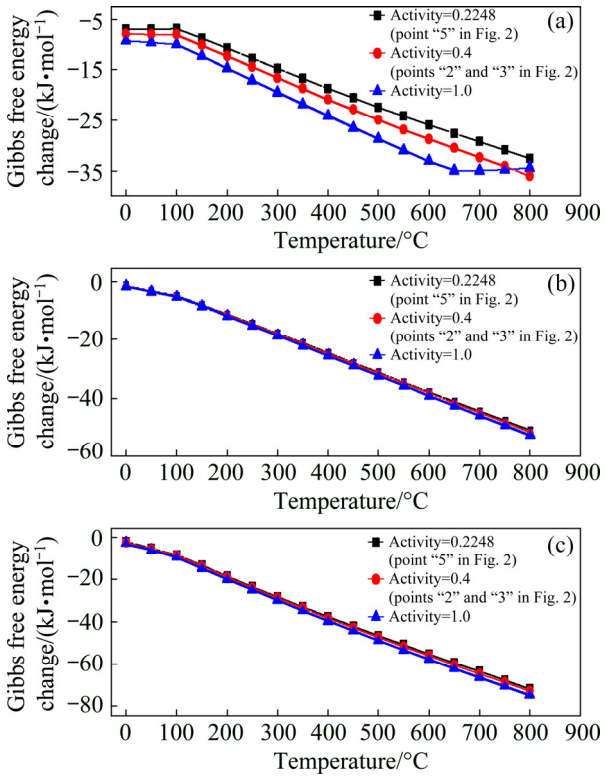

Fig. 5 Gibbs free energy changes with temperature for Sb_2O_3 in solid solutions in original dust reacted with CuS and S by assuming these solid solutions being ideal solid solution: (a) Eq. (8); (b) Eq. (10); (c) Eq. (12)

The calculations were performed on a mixture of 1 mol Sb_2O_3 and 2 mol As_2O_3 with variable amounts of CuS in the temperature range of 300−450 °C under an inert atmosphere at a pressure of 101.325 kPa. The phases of Sb_2S_3(s) [23], Cu_2S(s), As_2O_3(l), SbO_2(s), Sb_2O_3(s) and As_2S_3(l) are assumed to be present in the roasted products, and the phase of As_4O_6(g) is deemed to be volatilized and goes into the off-gas. The results of their equilibrium are presented in Fig. 6. It is noteworthy that massive Sb_2S_3(g) is generated in the original results given by FactSage 7.0, which differs obviously from the research of PADILLA et al [24]. Then further combined with our previous research [33], Sb_2S_3(g) is revised into Sb_2S_3(s) in the equilibrium results. When the CuS amount is less than 9 mol, As exists mainly in forms of As_2O_3(l) and As_4O_6(g). The As_2S_3(l) phase appears at a CuS amount of 9 mol, and it originates from the sulfidation of the As oxide (Eqs.(11) and (13)). The amount of Sb_2S_3(s) remains nearly constant when the CuS amount exceeds 9 mol. This seems to support the sulfidation of the antimony phase being

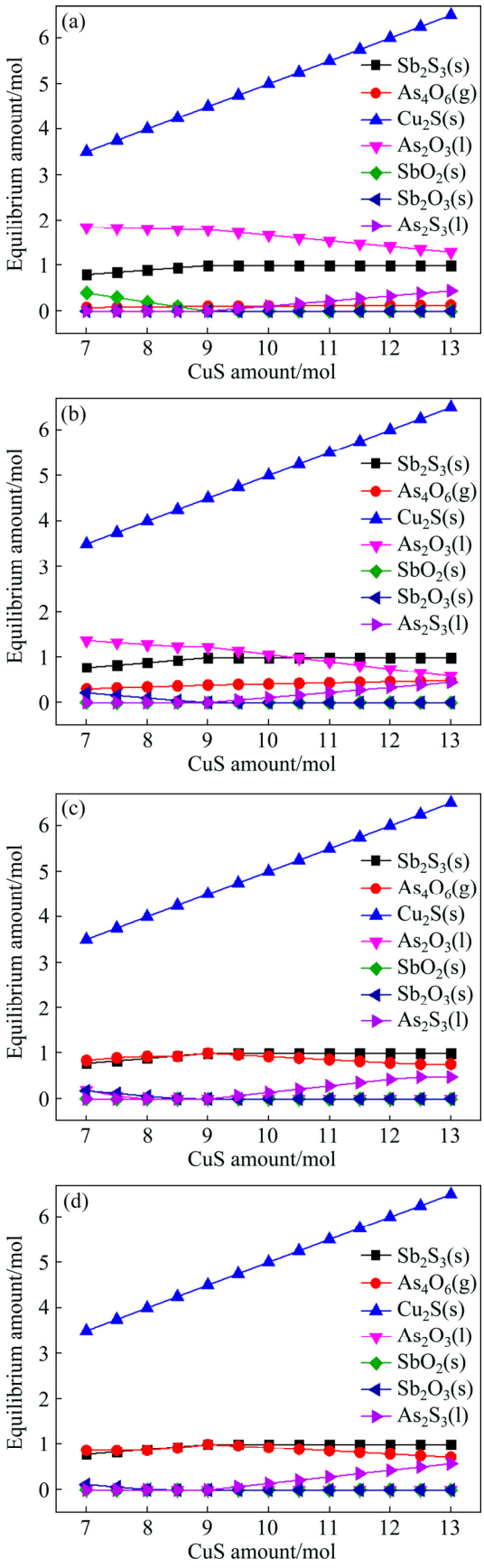

Fig. 6 Equilibrium amounts of species in roasted products as function of temperature and CuS amount: (a) 300 °C; (b) 350 °C; (c) 400 °C; (d) 450 °C

completed at a CuS amount of 9 mol and the sulfidation of the subsequent arsenic phases, which is due to the more negative standard Gibbs free energy changes of Eqs. (10) and (12) than those of Eqs. (11) and (13). In addition, the amount of As_4O_6(g) increases acutely with temperature, which is propitious for the separation of arsenic and antimony.

As mentioned above, the selective oxidation−sulfidation of the Sb phases from arsenic−antimony-bearing dusts and the As volatilization in form of As_4O_6 (g) could be achieved by controlling the temperature and CuS amount, in which the temperature and CuS amount should be controlled at 400−450 °C and 9 mol, respectively, due to thermodynamics.

4 Results and discussion

4.1 Separation of arsenic

The mixtures of CuS and the dust in a proper ratio were roasted in the temperature range of 300−450 °C to investigate the effects on the volatilization rates of arsenic and antimony. The roasting time and N_2 flow rate were fixed at 100 min and 30 mL/min, respectively. Besides, a series of blank experiments without CuS addition were also carried out under the same condition.

All the experiments under the same conditions were repeated three times, and each set of data in Figs. 7 and 8 are the average values of these three repeated measurements. Figure 7 shows that an increase in temperature improves the volatilization of both arsenic and antimony on the whole. To be specific, the arsenic volatilization rate reaches a maximum at 400−425 °C and then remains nearly constant. The antimony volatilization rate changes slightly at 300−400 °C and then increases sharply with a continuing rise in temperature. Specially, the arsenic volatilization rate decreases slightly with temperature from 375 to 400 °C when α is less than 130%. The reason for this is that the $(Sb,As)_2O_3$ phase in the original dust is transformed to the As−Sb−S phase and the corresponding arsenic compounds vapor pressure decreases. This will be investigated by EPMA analysis in the following section. Without CuS addition, Fig. 8 shows that the arsenic volatilization rate is relatively low, the reason for which might be due to a formation of coexistent phase (As−Sb−O) which inhibits the As volatilization. It will be also investigated by XRD and EPMA analysis in the following section.

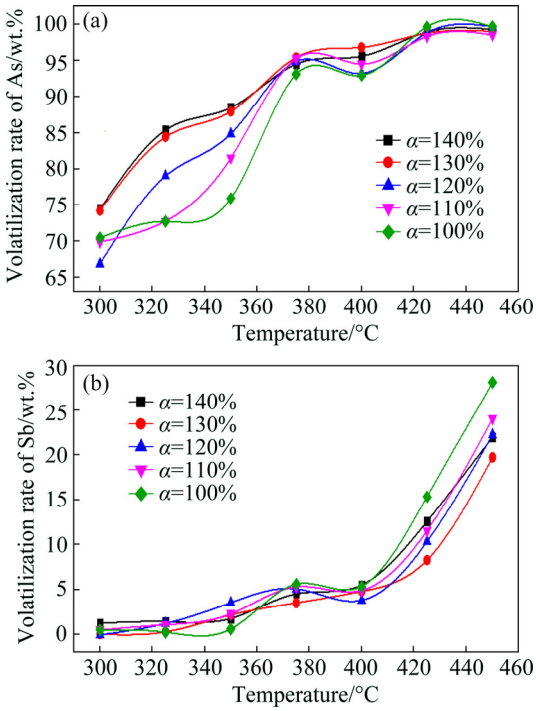

Fig. 7 Effects of roasting temperature and CuS amount on volatilization rate of arsenic and antimony

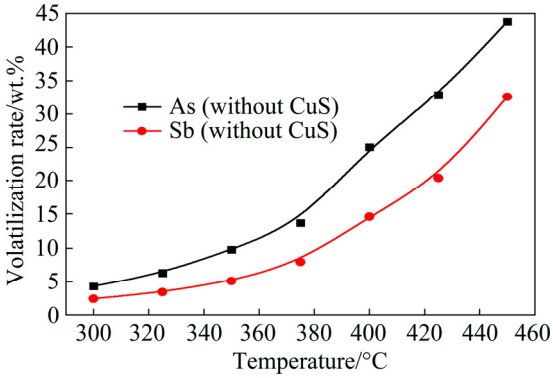

Fig. 8 Effects of roasting temperature on volatilization rate of arsenic and antimony without CuS addition

The CuS plays a dual role on the volatilization of antimony. The antimony volatilization rate decreases with the CuS amount from 100% to 130% and then increases with the CuS amount from 130% to 140%. The reason for this might be that Sb_2S_3 and Sb_2O_4 are generated with a CuS amount from 100% to 130% and neither of them is volatile. However, the generated Sb_2S_3 and Sb_2O_4 are transformed into As−Sb−S and Sb_4O_6 when the CuS amount is greater than 130%, causing Sb to be volatilized in the form of Sb_4O_6. These will also be investigated by XRD and EPMA analysis in the

following section.

The optimum parameters are selected as a roasting temperature of 400 °C and a CuS amount of 130% to increase the separation efficiency of arsenic and antimony. Their volatilization rates can reach 97.80 wt.% As and only 8.29 wt.% Sb, respectively.

4.2 Analysis of mechanism of arsenic separation

It is important to establish a qualitative measurement of the mechanism to confirm the roasting process.

The broadening of the XRD peak in Fig. 9(a) indicates amorphous nature of the roasted calcine without CuS addition, and Fig. 9(b) demonstrates that this amorphous roasted calcine is mainly complex multi-phase crystal system containing varying amounts of As and Sb (in combination with oxygen). It restricted the arsenic volatilization obviously.

The mineral compositions of the roasted calcines with a CuS amount of 130% at different roasting temperatures were analyzed by XRD and the results are shown in Fig. 10(a). The broadening of the XRD peaks at 300 °C in Fig. 10(a) indicates the amorphous nature of the roasted calcine, and Fig. 10(b) shows that this amorphous solid is mainly composed of As−Sb−O and Sb−S phases [26−28]. From a comparison of Fig. 2 and Fig. 10(b), it can be concluded that the most dissociative state As_2O_3 has been removed and the amount of combined state of As_2O_3 ($(Sb,As)_2O_3$ in Fig. 1) also clearly decreases. The destruction of the $(Sb,As)_2O_3$ structures in the original dust might be due to the oxidizing action of Cu^{2+} in CuS [29]. The structure of the $(Sb,As)_2O_3$ compound is further destroyed when the temperature is increased to 400 °C, as seen by comparing Fig. 10(c) to Fig. 10(b), in which the Sb component is further oxidized and sulfurized into Sb_2O_4 and Sb_2S_3 (Fig. 10(a)), respectively, by CuS and S through Eqs. (8), (10) and (12). Sb_2O_4 and Sb_2S_3 stay in the roasted calcine, which results in the low antimony volatilization rate as shown in Fig. 7. Meanwhile, the As component in $(Sb,As)_2O_3$ is released and volatilizes in the form of As_4O_6, resulting in a sharp increase in the arsenic volatilization rate between 300 and 400 °C (Fig. 7).

In addition, when α is lower than 130%, the arsenic sulfide could be formed through Eqs. (11) and (13) and combined with Sb_2S_3, generating a coexistent phase of As−Sb−S [27] at 400 °C. This can be confirmed by the EPMA−EDS result in Fig. 11 (α=110%). This As−Sb−S specie is difficult to volatilize at 400 °C, and it causes a slight decrease in the arsenic volatilization rate as the temperature increases from 375 to 400 °C.

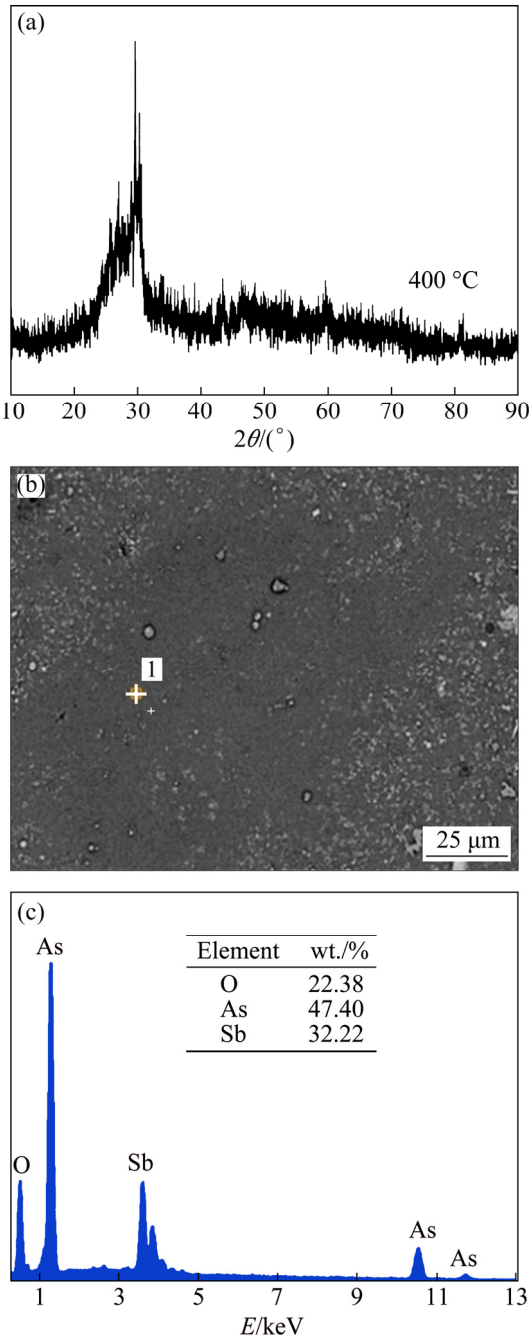

Fig. 9 XRD pattern (a), EPMA analysis (b) and EDS analysis (c) of roasted residue at 400 °C without CuS addition

The XRD patterns of roasted calcines with different CuS amounts at 425 °C are shown in Fig. 12. It shows that the peak intensity of Sb_2O_4

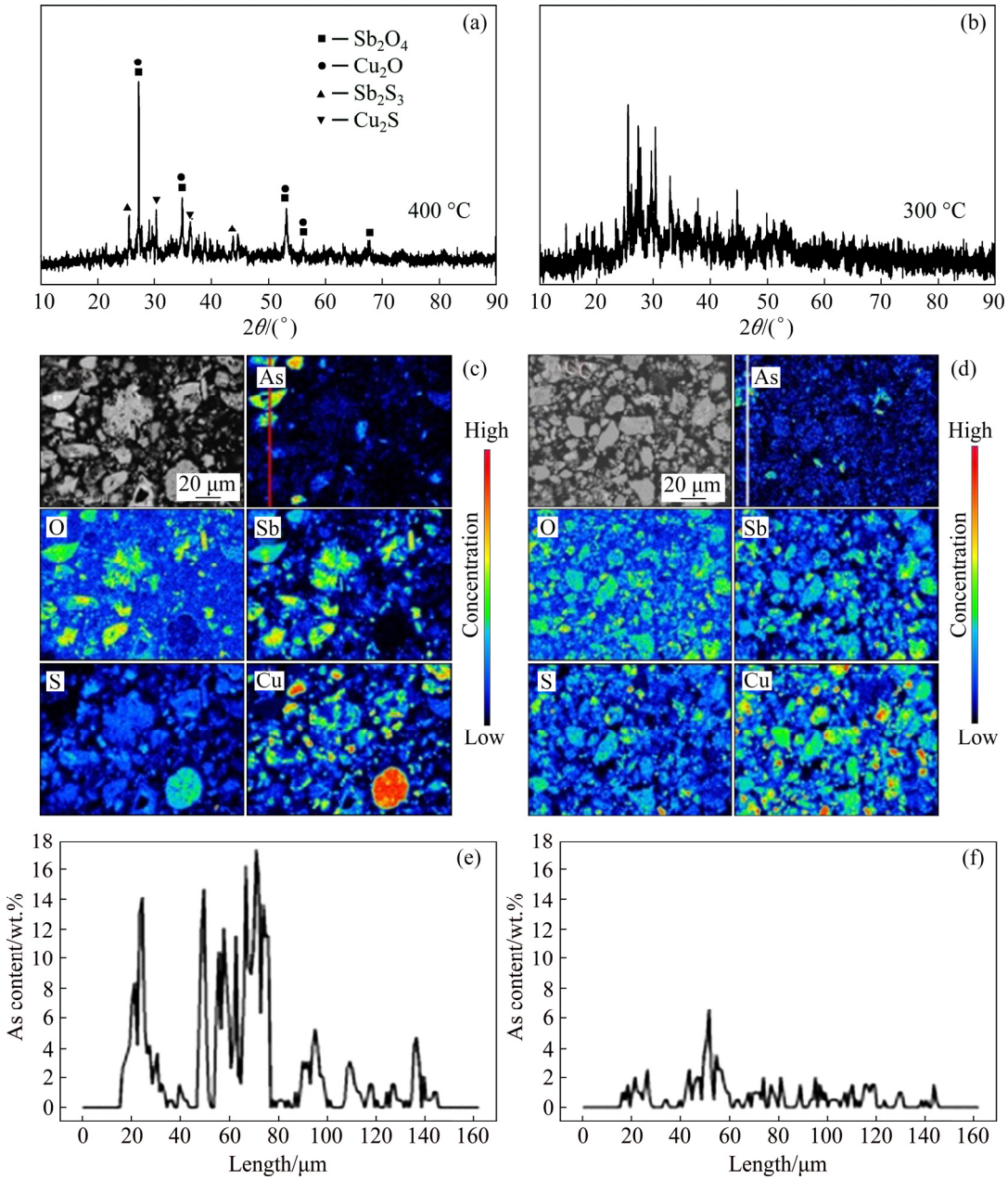

Fig. 10 XRD patterns (a, b), EPMA analyses (c, d), and line scanning analyses (e, f) of roasted residue at 300 °C (a, c, e) and 400 °C (b, d, f)

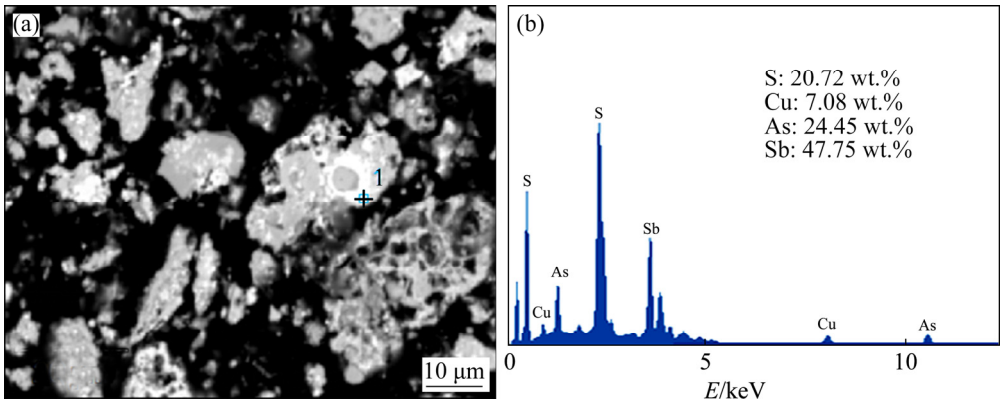

Fig. 11 EPMA−EDS analyses of roasted residue at 400 °C (α=110%)

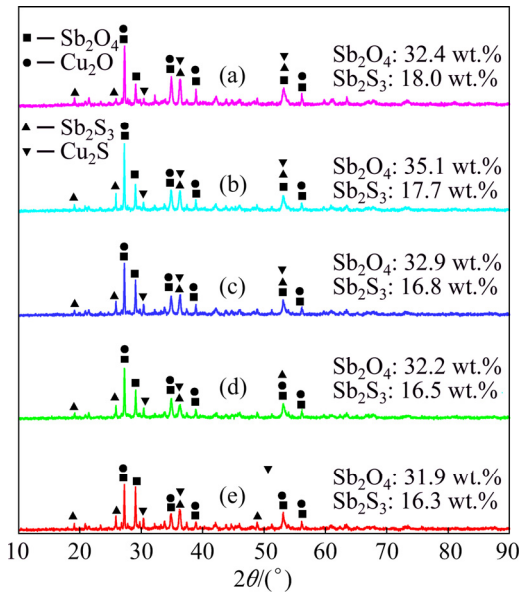

Fig. 12 XRD patterns of roasted residues with different CuS amounts at 425 °C: (a) α=140%; (b) α=130%; (c) α=120%; (d) α=110%; (e) α=100%

and Sb_2S_3 increases gradually, with α ranging from 100% to 130% and then Sb_2O_4 peak decreases when α is above 130%, which occurs because Sb_2O_4 is reduced into volatile Sb_4O_6 by the "S" component in CuS through Eq. (14) at a higher α value. This results in an increase in the antimony volatilization rate at 400−450 °C in Fig. 7. Figure 13 shows that Eq. (14) can proceed by increasing temperature and decreasing the partial pressures (P) of Sb_4O_6(g) and SO_2(g). The partial pressures of Sb_4O_6(g) and SO_2(g) are low and always decreasing in the roasting process due to their strong volatility.

$$4CuS(s)+10Sb_2O_4(s)=5Sb_4O_6(g)+2Cu_2O(s)+4SO_2(g) \quad (14)$$

The volatile matter in the water-cooled condenser (device No. 10 in Fig. 2) was collected, and its XRD pattern is shown in Fig. 14. It is shown that the volatile matter is mainly composed of As_2O_3, accompanied by a small amount of Sb_2O_3. The volatile matter, containing a high amount of As_2O_3, could be used to prepare ferric arsenate after it was oxidized, with this treatment rendering the vapor harmless. In addition, after being roasted with CuS, Sb_2O_3 and $(Sb,As)_2O_3$ in the original arsenic−antimony-bearing dust are transformed to Sb_2O_4 and Sb_2S_3 retaining in the roasted calcine, and meanwhile CuS is changed into Cu_2O and Cu_2S. Sb could be separated and recovered in the form of

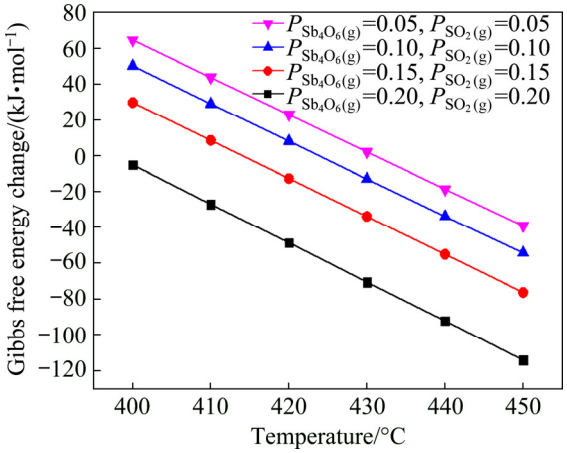

Fig. 13 Gibbs free energy changes of Eq. (14) with temperature under different $P_{Sb_4O_6(g)}$ and $P_{SO_2(g)}$

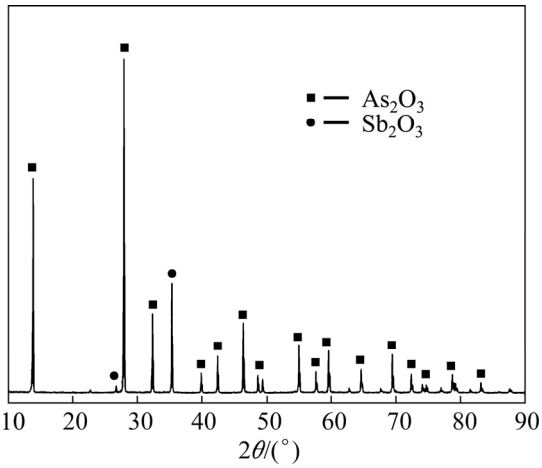

Fig. 14 XRD pattern of product in water-cooled condenser (device No. 10 in Fig. 2)

Sb_4O_6 from the Cu-containing roasted calcine through an oxidation−reduction process [34].

The thermodynamic behavior of As and Sb phases in the dust during the roasting process is summarized in Fig. 15. When the temperature is lower than 400 °C, most of Sb_2O_3 is oxidized and sulfurized to Sb_2O_4 and Sb_2S_3 by CuS and/or the decomposition products of CuS, and the structure of $(Sb,As)_2O_3$ in the original dust is destroyed via the oxidizing action of the Cu^{2+} in CuS. As a result, the volatilization rate of arsenic increases with the CuS amount accompanied by the antimony volatilization rate being lower than 5 wt.%. Increasing the temperature over 400 °C, As_2O_3 could be sulfurized to As_2S_3 and combined with Sb_2S_3 generating a coexistent phase of As−Sb−S with CuS amount of 110%−130%, which antagonizes the arsenic volatilization. In addition, the generated Sb_2O_4

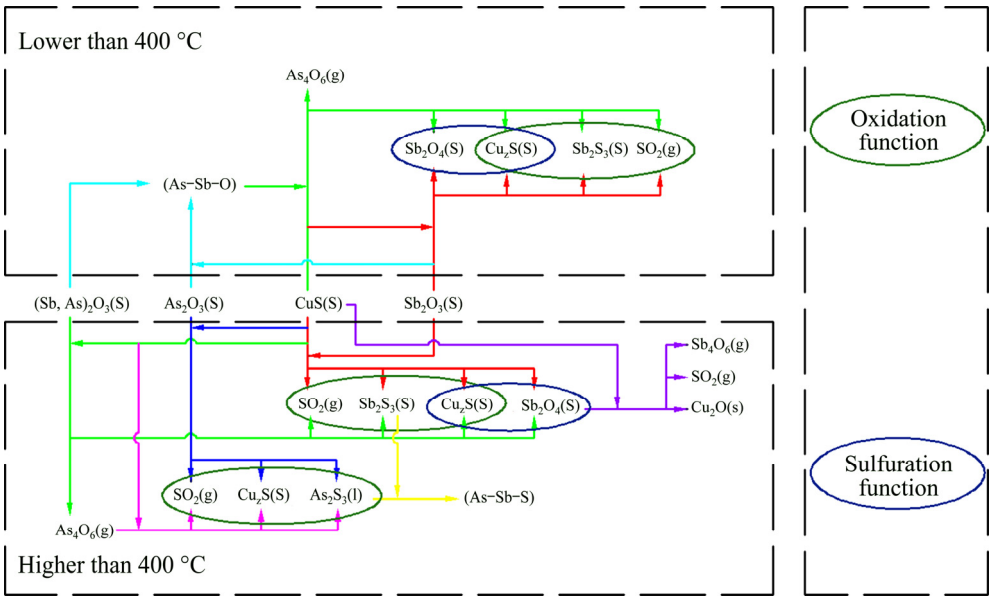

Fig. 15 Thermodynamic behavior of As and Sb phases in dust during oxidation−sulfidation roasting process using CuS

could be reduced into volatile Sb_4O_6 by the S component in CuS and causes the antimony volatilization rate increase.

5 Conclusions

(1) The effective removal of arsenic from arsenic−antimony-bearing dust through a selective oxidation−sulfidation roasting process using CuS was feasible. The factors of the roasting temperature and CuS amount played significant roles on the separation of arsenic and antimony.

(2) Both the thermodynamic analysis and experimental results showed that the oxidation and sulfidation of Sb_2O_3 occurred prior to those of As_2O_3, in which Sb was transformed into Sb_2O_4 and Sb_2S_3 that stayed in the roasted calcine while As was volatilized in the form of As_4O_6. The CuS played an active role in the separation of arsenic because the structure of $(Sb, As)_2O_3$ in the original dust could be destroyed through the oxidizing action of Cu^{2+} in CuS and As was released in the form of As_4O_6.

(3) When the roasting temperature and CuS amount were above 400 °C and 130%, respectively, the generated Sb_2O_4 could be reduced to volatile Sb_4O_6 by the S component in CuS, causing the rate of antimony volatilization to increase. To increase the As removal rate and reduce the loss of Sb, the optimum conditions were established as a roasting temperature of 400 °C with a CuS amount of 130%. After roasting under these conditions, the volatilization rates of arsenic and antimony reached 97.80 wt.% and only 8.29 wt.%, respectively.

References

[1] HENCKENS M L C M, DRIESSEN P P J, WORRELL E. Metal scarcity and sustainability, analyzing the necessity to reduce the extraction of scarce metals [J]. Resources, Conservation and Recycling, 2014, 93(11): 1−8.

[2] MONARREZ-CORDERO B, AMEZAGA-MADRID P, ANTUNEZ-FLORES W, LEYVA-PORRAS C, PIZA-RUIZ P, MIKI-YOSHIDA M. Highly efficient removal of arsenic metal ions with high superficial area hollow magnetite nanoparticles synthetized by AACVD method [J]. Journal of Alloys and Compounds, 2014, 586: S520−525.

[3] SINGH P, SHARMA S, CHAUHAN K, SINGHAL R K. Fabrication of economical Thiol-tethered bifunctional iron composite as potential commercial applicant for arsenic sorption application [J]. Industrial & Engineering Chemistry Research, 2018, 57: 12959−12972.

[4] SUN Bo, ZHAI Hao, ZHANG Li-bing, ZHANG Chun-xue, WU Xin-shi. Removal of trace arsenic based on biomimetic separation [J]. Industrial & Engineering Chemistry Research, 2015, 54: 396−403.

[5] LI Yi-ran, WANG Jun, LUAN Zhao-kun, LIANG Zhen. Arsenic removal from aqueous solution using ferrous based red mud sludge [J]. Journal of Hazardous Materials, 2010, 177(1−3): 131−137.

[6] TANG Shi-jia, GAO Guang-ming, PENG En-sheng, SUN Zhen-jia. Fractal feature of western fracture zone in Xikuangshan antimony mine and its geological significance [J]. Journal of Central South University of Technology, 2000,

7 (4): 212−215.

[7] SHAWABKEH R A. Hydrometallurgical extraction of zinc from Jordanian electric arc furnace dust [J]. Hydrometallurgy, 2010, 104: 61−65.

[8] ELLNER M. Crystal chemical investigation of the solid solutions of antimony and bismuth in palladium and platinum [J]. Journal of Alloys and Compounds, 2007, 436 (1−2): 78−81.

[9] LI Lei, ZHANG Ren-jie, LIAO Bin, XIE Xiao-feng. Separation of As from As and Sb contained smoke dust by selective oxidation [J]. The Chinese Journal of Process Engineering, 2014, 14 (1): 71−77. (in Chinese)

[10] LI Yu-hu, LIU Zhi-hong, LI Qi-hou, LIU Fu-peng, LIU Zhi-yong. Alkaline oxidative pressure leaching of arsenic and antimony bearing dusts [J]. Hydrometallurgy, 2016, 166: 41−47.

[11] WANG Jiang-sheng. Reclaiming valuable metals from copper converter dust [J]. Copper Industrial Engineering, 2005, 1: 27−28. (in Chinese)

[12] KASHIWAKURA S, OHNO H, MATSUBAE-YOKOYAMA K, KUMAGAI Y, KUBO H, NAGASAKA T. Removal of arsenic in coal fly ash by acid washing process using dilute H_2SO_4 solvent [J]. Journal of Hazardous Materials, 2010, 181: 419−425.

[13] GUO Xue-yi, SHI Jing, YI Yu, TIAN Qing-hua, LI Dong. Separation and recovery of arsenic from arsenic-bearing dust [J]. Journal of Environmental Chemical Engineering, 2015, 3: 2236−2242.

[14] GUO Xue-yi, YI Yu, SHI Jing, TIAN Qing-hua. Leaching behavior of metals from high-arsenic dust by NaOH−Na_2S alkaline leaching [J]. Transactions of Nonferrous Metals Society of China, 2016, 26: 575−580.

[15] MONTENEGRO V, SANO H, FUJISAWA T. Recirculation of high arsenic content copper smelting dust to smelting and converting processes [J]. Minerals Engineering, 2013, 49: 184−189.

[16] JIANG Xue-xian, HE Gui-xiang, LI Xue-guang, LU Jing. Experimental research on dearsenization of high arsenic fume [J]. Hydrometallurgy of China, 2010, 29: 199−202. (in Chinese)

[17] VIRCIKOVA E, HAVLIK M. Removing As from converter dust by a hydrometallurgical method [J]. The Journal of The Minerals, Metals & Materials Society, 1999, 51: 20−23.

[18] LI Yu-hu, LIU Zhi-hong, LI Qi-hou, ZHAO Zhong-wei, LIU Zhi-yong, ZENG Li. Removal of arsenic from Waelz zinc oxide using a mixed NaOH−Na_2S leach [J]. Hydrometallurgy, 2011, 108: 165−170.

[19] SULLIVAN C, TYRER M, CHESSEMAN C R, GRAHAM N J. Disposal of water treatment wastes containing arsenic—A review [J]. Science of the Total Environment, 2010, 408: 1770−1778.

[20] LI Yu-hu, LIU Zhi-hong, LI Qi-hou, ZHAO Zhong-wei, LIU Zhi-yong, ZENG Li, LI Li. Removal of arsenic from arsenate complex contained in secondary zinc oxide [J]. Hydrometallurgy, 2011, 109: 237−244.

[21] ZHANG Hui-bin, LIU Xin-li, JIANG Yao, GAO Lin, YU Lin-ping, LIN Nan, HE Yue-hui, LIU C T. Direct separation of arsenic and antimony oxides by high-temperature filtration with porous FeAl intermetallic [J]. Journal of Hazardous Materials, 2017, 338: 364−371.

[22] YUAN Hai-bin, ZHU Yu-yan, ZHANG Ji-bin. Process of high-arsenic dust containing tin volatilization from DC submerged arc furnace [J]. Journal of Central South University, 2013, 44: 2200−2205. (in Chinese)

[23] ARACENA A, JEREZ O, ANTONUCCI C. Senarmontite volatilization kinetics in nitrogen atmosphere at roasting/melting [J]. Transactions of Nonferrous Metals Society of China, 2016, 26: 294−300.

[24] PADILLA R P, RAMIREZ G, RUIZ M C. High-temperature volatilization mechanism of stibnite in nitrogen-oxygen atmospheres [J]. Metallurgical and Materials Transactions B, 2010, 41: 1284−1292.

[25] TANG Hai-bo, QIN Qing-wei, GUO Yong, ZHENG Xin, XUE Ping, LI Guang-qiang. Pretreatment of high arsenic and antimony smelting dust for arsenic removal using roasting process [J]. Conservation and Utilization of Mineral Resources, 2014, 3: 35−38. (in Chinese)

[26] BROOKS G A, RANKIN W J, GRAY N B. Thermal separation of arsenic and antimony oxides [J]. Metallurgical and Materials Transactions B, 1994, 25: 873−884.

[27] MAUSER J E. Heteronuclear compounds of arsenic and antimony [J]. Metallurgical and Materials Transactions B, 1982, 13: 511−513.

[28] BROOKS G A, RANKIN W J. Solid-solution formation between arsenic and antimony oxides [J]. Metallurgical and Materials Transactions B, 1994, 25: 865−871.

[29] ZHONG Da-peng, LI Lei, TAN Cheng. Separation of arsenic from the antimony-bearing dust through selective oxidation using CuO [J]. Metallurgical and Materials Transactions B, 2017, 48: 1308−1314.

[30] FACTSAGE 7.0: FactPS-FACT Pure Substances Database, Thermfact/CRCT and GTT Technologies, 2015.

[31] NAFEES M, IKRAM M, ALI S. Thermal behavior and decomposition of copper sulfide nanomaterial synthesized by aqueous sol method [J]. Digest Journal of Nanomaterials and Biostructures, 2015, 10: 635−641.

[32] JIANG Xu-chuan, XIE Yi, LU Jun, HE Wei, ZHU Li-ying, QIAN Yi-tai. Preparation and phase transformation of nanocrystalline copper sulfides (Cu_9S_8, Cu_7S_4 and CuS) at low temperature [J]. Journal of Materials Chemistry, 2000, 10: 2193−2196.

[33] TAN Cheng, LI Lei, ZHONG Da-peng, WANG Hua, LI Kong-zhai. Separation of arsenic and antimony from dust with high content of arsenic by a selective sulfidation roasting process using sulfur [J]. Transactions of Nonferrous Metals Society of China, 2018, 28: 1027−1035.

[34] ZHONG Da-peng, LI Lei, TAN Cheng. Recovery of antimony from antimony-bearing dusts through reduction roasting process under CO−CO_2 mixture gas atmosphere after firstly oxidation roasted [J]. Journal of Central South University, 2018, 25: 1904−1913.

添加硫化铜选择性氧化-硫化焙烧分离砷锑烟尘中的砷

钟大鹏，李 磊

昆明理工大学 复杂有色金属资源清洁利用国家重点实验室，
冶金节能减排教育部工程研究中心，冶金与能源工程学院，昆明 650093

摘 要：以 CuS 为添加剂对砷锑烟尘进行焙烧可实现其中砷的有效脱除，过程中 Sb 转化为 Sb_2O_4 与 Sb_2S_3，保留在底物中，As 则以 As_4O_6 形式挥发。借助 XRD、EPMA 和 SEM−EDS 等表征手段，对焙烧温度与 CuS 加入量对砷分离效率的影响规律进行研究。结果表明，CuS 对砷的分离有促进作用，其原因为：CuS 可将$(Sb,As)_2O_3$ 固溶体结构破坏，使其中 As 以 As_4O_6 形式挥发脱除。焙烧温度为 400 °C、CuS 用量为 130%时，砷锑烟尘中砷的挥发率高达 97.80%，锑挥发损失率仅为 8.29%。同时，高砷挥发物被氧化后可用于制备砷酸铁以实现其无害化处理。

关键词：砷锑烟尘；砷锑分离；CuS；物相转变；废物利用

(Edited by Xiang-qun LI)